J Therm Anal Calorim
DOI 10.1007/s10973-016-5953-1

Studies on some metal complexes of a quinoxaline based unsymmetrical ONNO donor ligand

Synthesis, spectral characterization, thermal, in vitro biological and DFT studies

C. Justin Dhanaraj[1] · Jijo Johnson[1]

Received: 4 March 2016 / Accepted: 8 November 2016

Abstract Co(II), Ni(II), Cu(II) and Zn(II) complexes of an unsymmetrical tetradentate ONNO donor ligand, 3-(-(3-(-1-(2-hydroxyphenyl)ethylideneamino)propylimino)methyl) quinoxalin-2(1*H*)-one (**L**) have been synthesized and characterized by elemental analysis, molar conductance, magnetic susceptibility measurements, FTIR, UV–Vis., mass and ^{1}H NMR spectral studies. ESR spectra of the Cu(II) complex under room (300 K) and liquid nitrogen temperature (77 K) were also recorded. Thermal behavior of the newly synthesized ligand and its metal complexes was assessed by TG–DTG analysis. All the complexes are found to be mononuclear. Crystallinity, average grain size and unit cell parameters were determined from powder X-ray diffraction study. Electrochemical behavior of the compounds was examined by cyclic voltammetry technique. The in vitro antimicrobial screening of the unsymmetrical ligand and corresponding metal chelates was tested against some bacterial strains (*E. coli*, *K. pneumoniae*, *S. pneumoniae* and *S. aureus*) and fungal strains (*A. niger*, *A. flavus*, *P. chrysogenum* and *R. stolonifer*). The in vitro antioxidant and anticancer activities of the compounds were also evaluated. DFT studies were done to optimize the structure of the compounds and to calculate nonlinear optical properties of the compounds.

Electronic supplementary material The online version of this article (doi:10.1007/s10973-016-5953-1) contains supplementary material, which is available to authorized users.

✉ C. Justin Dhanaraj
c.justindhanaraj@gmail.com

[1] Department of Chemistry, University College of Engineering, Nagercoil (Anna University Constituent College), Konam, Nagercoil, Tamil Nadu 629 004, India

Published online: 29 November 2016

Graphical Abstract

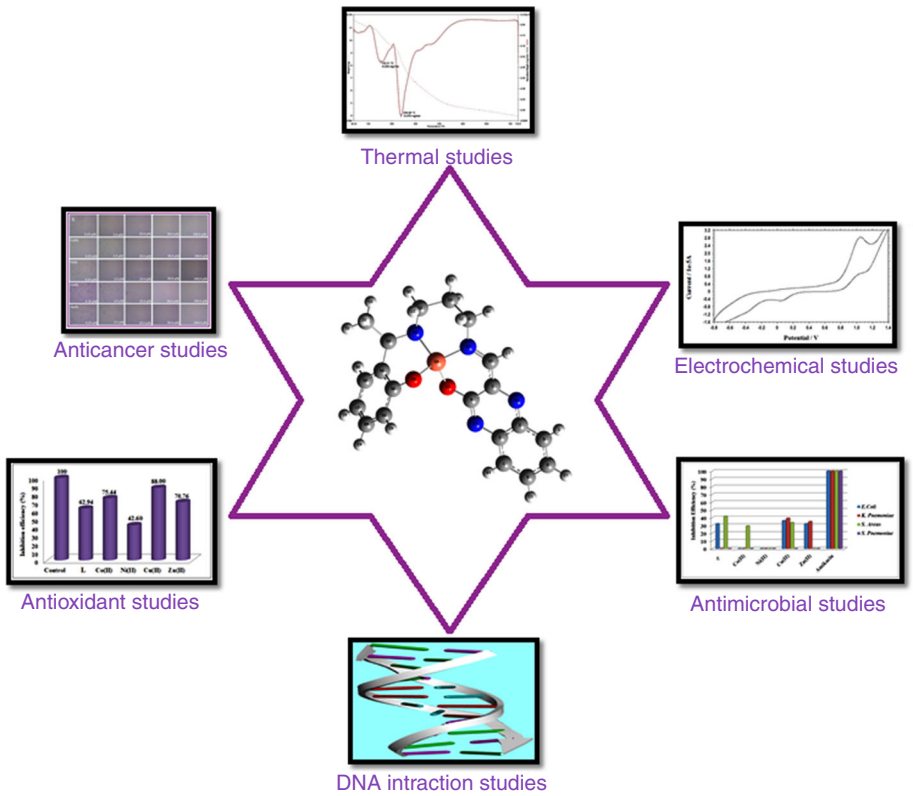

Keywords TG–DTG · Antimicrobial · Antioxidant · MTT assay · Nonlinear optical properties

Introduction

Schiff bases have a double bond (R–C=N) and synthesized by the condensation of primary amines and active carbonyl groups (aldehydes/ketones). Schiff bases display fascinating properties. They act as metal complexing agents in biological systems, catalyst carriers, corrosion inhibitors, thermostable materials and coloring agents. They are also widely used as preparatory materials in the synthesis of important antifungals, antibiotics, antitumors and antiallergics due to their biological activities [1]. It has been suggested that the azomethine linkage is responsible for the biological activities of Schiff bases [2]. Metal complexes of Schiff base ligand have shown desirable enhancement in their biological activities after chelation as compared to un-coordinated Schiff base ligand [3].

The modern era of metal-based anticancer drugs began with the innovation of the antitumor properties of cisplatin. Presently, cisplatin, oxaliplatin and carboplatin are among the most important chemotherapeutics used against a variety of cancers [4]. Despite its success, clinical use of cisplatin is limited due to acquired and intrinsic resistance of cancer cells to the drug and its high toxicity to some normal cells. Therefore, there exists an enormous interest to improve the design of metallodrugs having reduced toxicity and a high spectrum of activity, especially drugs that would show activity against cell lines resistant to cisplatin [5].

Quinoxaline derivatives and their metal chelates show some remarkable biological activities [6–10]. Literature survey [11] reveals that no reports are available on unsymmetrical Schiff base ligands incorporating quinoxaline derivatives. It is also noticed that the biological (especially anticancer activities) and molecular modeling studies of quinoxaline-based Schiff base transition metal complexes are not much explored.

By considering the above facts, an attempt has been made to develop some novel bioactive metal complexes of an ONNO donor unsymmetrical Schiff ligand including quinoxaline, *o*-hydroxyacetophenone and 1,3-diaminopropane. Herein we report the synthesis, spectral characterization, thermal, electrochemical, powder XRD, in vitro antimicrobial, DNA cleavage, antioxidant and anticancer activities and DFT studies of Co(II), Ni(II), Cu(II) and Zn(II) complexes of a Schiff base ligand having azomethine (HC=N) and imine (C=N) donor sites.

Experimental

Materials

The chemicals used were of AnalaR grade except *o*-phenylenediamine and used as received without further purification. *O*-phenylenediamine (LR grade, Loba Chemie, India) was purified through recrystallization from hot methanol. Hydrazine hydrate, bromine, calcium carbonate, *o*-hydroxyacetophenone, 1,3-diaminopropane, metal(II) acetates and solvents were bought from Merck. Sodium pyruvate and glacial acetic acid were bought from SRL PVT. Ltd., India.

Instrumental

Elemental analyses of ligand and its metal complexes were carried out using Perkin Elmer elemental analyzer. The metal contents in the metal complexes were determined by standard EDTA titration. Molar conductance of the complexes was measured using Systronic, MK-509 digital conductivity meter. FTIR spectra were recorded using Brucker ALPHA-D spectrophotometer by KBr pellet method from 4000–400 cm^{-1}. ^{1}H NMR and ^{13}C NMR spectra of ligand and its Zn(II) complex were recorded with Brucker 700 MHz spectrometer using $CDCl_3$ solvent with TMS as internal standard. DART-MS spectra were recorded on a JEOL-Accu TOF JMS mass spectrometer. Magnetic moments were measured by Guoy method and corrected for diamagnetism of the component using Pascal's constants. Electronic absorption spectra were recorded on Lasany UV–visible double-beam spectrophotometer (Model No. I-2902) at the wavelength range 190–1100 nm. ESR spectra of the [Cu(**L**)] complex were recorded at 300 and 77 K in DMSO solution using Varian, USA E-112 ESR spectrometer using tetracyanoethylene (TCNE) as g-marker. Thermal analysis was carried out under nitrogen and air atmospheres at a heating rate of 10 °C per minute using PerkinElmer Diamond TG/DTA analyzer. Alumina crucibles were used for recording thermogravimetric curves. The metal content present in the final residues obtained from the thermal analysis in air atmosphere was also determined using a Shimadzu AA 7000 Atomic Absorption Spectrometer. Cyclic voltammetry measurements were done using electrochemical analyzer CH instrument electrochemical workstation (Model 650 C) using a glassy carbon working electrode (GCE) and Ag/AgCl reference electrode and platinum counter electrode. Powder XRD studies were carried out using XPERT-PRO, X-ray diffractometer system.

Synthesis of ligand

The unsymmetrical Schiff base ligand **L** was synthesized by the following procedure. The Schiff base half unit 2-(1-(3-aminopropylimino)ethyl)phenol was prepared by following the method reported earlier [12, 13] with slight modification. To the methanolic solution of *o*-hydroxyacetophenone (5.0 mmol), a methanolic solution of 1,3-diaminopropane (7.5 mmol) was added drop by drop from a dropping funnel. To the above mixture, few drops of Con. H_2SO_4 (as dehydrating agent) was added and stirred with heating for ~2 h. The resultant solution was cooled to room temperature, and the fluorescent green-colored product 2-(1-(3-aminopropylimino)ethyl)phenol formed was washed with ether and cold water. The product was then filtered and dried over anhydrous calcium chloride. The product obtained was recrystallized from hot methanol.

In the second step, to the solution of 3-hydroxyquinoxaline-2-carboxaldehyde (5.0 g, 28.7 mmol, in 500 mL distilled water), 3–4 drops of conc. HCl was added to acidify the aqueous solution. An alcoholic solution of 2-(1-(3-aminopropylimino)ethyl)phenol (7.09 g, 28.7 mmol, in 50 mL methanol) was added to the above solution dropwise with constant stirring. The dark red-colored Schiff base precipitated was filtered, washed with petroleum ether and dried over anhydrous calcium chloride. The ligand was recrystallized from hot methanol.

Synthesis of metal complexes

The Co(II), Ni(II), Cu(II) and Zn(II) complexes of **L** was prepared by the following procedure. **L** (2 mmol) dissolved in 50 mL of methanol was mixed with solution of metal acetates (2 mmol) in 50 mL methanol and was stirred for ~6–8 h at 60–80 °C. The precipitate formed was filtered off, washed with cold methanol and dried in vacuum over anhydrous calcium chloride.

Biological studies

In vitro antimicrobial activity

In vitro antibacterial activities of **L** and its complexes were tested against two gram-negative (*E. coli* and *K. pneumoniae*) and two gram-positive (*S. pneumoniae* and *S. aureus*) bacterial strains by disk diffusion method [14]. The fungal species used for antifungal activity screening are *A. niger*, *A. flavus*, *P. chrysogenum* and *R. stolonifer*. Amikacin was used as standard antibacterial agent, and fluconazole was used as standard antifungal agent. The test organisms were grown on nutrient agar (Muller Hinton agar for bacteria and antimitotic agar for fungi) medium in petri plates. The

compounds were prepared in DMF and soaked in filter paper disks of 5 mm diameter and 1 mm thickness. The disks were placed on the previously seeded plates and incubated at 37 °C. The diameter of inhibition zone around each disk was measured after 24 h for bacterial and 72 h for fungal species. The antimicrobial activities of the compounds were established by calculating their activity index by using the following expression [15].

$$\text{Activity index } (A) = \frac{\text{Inhibition zone of compound (mm)}}{\text{Inhibition zone of standard drug (mm)}} \times 100 \quad (1)$$

DNA cleavage

The cleavage of supercoiled pUC18 DNA to its nicked circular and linear forms was studied by using agarose gel electrophoresis. pUC18 DNA (0.3 μg) was dissolved in 5 mmol L^{-1} Tris–HCl/50 mmol L^{-1} NaCl buffer (pH 7.2) and was treated with the complexes. The mixture was incubated at 37 °C for 1 h and then mixed with the loading buffer containing 25% bromophenol blue, 0.25% xylene cyanol and 30% glycerol. Each sample (10^{-3} M, 0.5 μL) was loaded into 1% (w/v) agarose gel. Electrophoresis was done for 2 h at 100 V in Tris–acetate–EDTA (TAE) buffer (pH 8.0). The gel was stained with ethidium bromide for 5 min after electrophoresis and then photographed under a UV transilluminator. In DNA cleavage experiment, H_2O_2 and DMSO were used as oxidizing and reactive oxygen species (ROS) scavenger, respectively. The DNA cleavage efficiency of the complexes was measured by determining the ability of the complexes to convert the supercoiled DNA to nicked circular form and linear form.

Superoxide anion scavenging activity

The scavenging effect of the compounds on superoxide anion radicals was estimated as follows: the reaction mixture contained 1 mL of riboflavin (3.3 × 10 mol L^{-1}), methionine (0.01 mol L^{-1}), 1 mL of nitro blue tetrazolium chloride (NBT, 4.6 × 10 mol L^{-1}) and phosphate buffer solution as solvent (0.05 mol L^{-1}, pH 7.8). After adding 1 mL of sample (mg/mL), the reaction mixture was illuminated at 4000 lx and 25 °C for 30 min. The absorbance of the reaction mixture was measured at 560 nm with a spectrophotometer, and the percentage of superoxide radical scavenging activity was calculated according to the following formula [16].

$$\%\text{ of super oxide anion scavenging activity} = \frac{(A_{\text{control}} - A_{\text{sample}})}{A_{\text{control}}} \times 100 \quad (2)$$

Hydrogen peroxide scavenging activity

The ability of the compounds to scavenge hydrogen peroxide was assessed by this method. A solution of H_2O_2 (40 mM) was prepared in phosphate buffer (0.1 M, pH 7.4). The compounds in DMF solution at the concentration of 10 mg/10 μL were added to H_2O_2 solution (0.6 mL), and the total volume was made up to 3 mL. The absorbance of the reaction mixture was recorded at 230 nm in a spectrophotometer. A blank solution containing phosphate buffer without H_2O_2 was prepared and used as control. The extent of H_2O_2 scavenging of the extracts was calculated using the following expression [17].

$$\%\text{ of } H_2O_2 \text{ scavenging activity} = \frac{(A_{\text{control}} - A_{\text{sample}})}{A_{\text{control}}} \times 100 \quad (3)$$

In vitro anticancer study

The human breast adenocarcinoma cell line (MCF7) was obtained from National Centre for Cell Science (NCCS), Pune, and grown in Eagle's minimum essential medium (EMEM) containing 10% fetal bovine serum (FBS). All the cells were maintained at 37 °C, 5% CO_2, 95% air and 100% relative humidity. The monolayer cells were detached with trypsin–ethylenediaminetetraacetic acid (EDTA) to make single-cell suspensions, and viable cells were counted using a hemocytometer and diluted with a medium containing 5% FBS to give final density of 1×10^5 cells/mL. Hundred microliters per well of cell suspension was seeded into 96-well plates at plating density of 10,000 cells per well and incubated at 37 °C, 5% CO_2, 95% air and 100% relative humidity. After 24 h, the cells were treated with serial concentrations of the test samples. They were initially dissolved in neat dimethylsulfoxide (DMSO) and diluted to twice the desired final maximum test concentration with serum-free medium. Additional fourfold and twofold serial dilutions were made to provide a total of five sample concentrations. Aliquots of 100 μL of these different sample dilutions were added to the appropriate wells already containing 100 μL of medium, giving the required final sample concentrations. Following drug addition, the plates were incubated for an additional 48 h at 37 °C, 5% CO_2, 95% air and 100% relative humidity. The medium without samples served as control, and triplicate was maintained for all concentrations. Tamoxifen was used as standard drug.

3-[4,5-Dimethylthiazol-2-yl]2,5-diphenyltetrazolium bromide (MTT) assay 3-[4,5-dimethylthiazol-2-yl]2,5-diphenyltetrazolium bromide (MTT) is a yellow water-soluble

tetrazolium salt. A mitochondrial enzyme in living cells, succinate dehydrogenase, cleaves the tetrazolium ring, converting the MTT to an insoluble purple formazan. Therefore, the amount of formazan produced is directly proportional to the number of viable cells. After 48 h of incubation, 15 µL of MTT (5 mg/mL) in phosphate-buffered saline (PBS) was added to each well and incubated at 37 °C for 4 h. The medium with MTT was then flicked off, and the formazan crystals formed were dissolved in 100 µL of DMSO, and absorbance at 570 nm was measured using a microplate reader. The percentage of cell inhibition was determined using the following formula [18, 19].

$$\%\,\text{of cell inhibition} = 100 - \text{Abs (sample)}/\text{Abs (control)} \times 100 \tag{4}$$

Using GraphPad Prism software, nonlinear regression graph was plotted between % cell inhibition and log concentration and IC_{50} values were determined.

DFT studies

The geometry optimization of the ligand and its metal complexes was carried out theoretically using Gaussian 09W program package [20] by DFT/B3LYP method. 6-31G(*d*,*p*) and LANL2DZ are the basis sets chosen. All computational process of ligand and metal complexes were made by using GaussView 5.0.8 software [21]. Here the B3LYP stands for Becke's three parameters exchange functional (B3) [22] in combination with the Lee–Yang–Parr correlation functional (LYP) [23]. 6-31G(*d*,*p*) is a popular polarized basis set which adds 'p' function to hydrogen atoms in addition to the 'd' functions on heavy atoms, while LANL2DZ is a basis set for post-third row atoms. This basis set uses effective core potential (ECP) in calculations [24]. The geometries of the metal complexes were fully optimized at B3LYP/GENECP level by using 6-31G(*d*,*p*) basis sets for C, H, N and O atoms and LANL2DZ basis sets for Co, Ni, Cu and Zn atoms in gas phase. GENECP is a keyword with the combination of 6-31G(*d*,*p*) and LANL2DZ standard basis sets. The atomic charge distributions of atoms in the compounds were determined by natural population analysis (NPA). The NPA calculations were made at B3LYP/LANL2DZ level [25].

According to Koopmans' theorem [26],

$$-E_{\text{HOMO}} = \text{IE} \tag{5}$$

$$-E_{\text{LUMO}} = \text{EA} \tag{6}$$

where IE and EA stands for ionization energy and electron affinity, respectively.

The absolute electronegativity (χ_{abs}) and absolute hardness (η) are related to IA and EA [27] and is given below (Eqs. 7 and 8).

$$\chi_{\text{abs}} = (\text{IE} + \text{EA})/2 = (E_{\text{HOMO}} + E_{\text{LUMO}})/2 \tag{7}$$

$$\eta = (\text{IE} - \text{EA})/2 = (E_{\text{HOMO}} - E_{\text{LUMO}})/2 \tag{8}$$

Another two important properties related to chemical potential (μ) [28] and hardness (η) are electrophilicity index (ω) and global softness (S). These values were calculated using Eqs. (9)–(11) [29].

$$\mu = -(E_{\text{HOMO}} + E_{\text{LUMO}})/2 \tag{9}$$

$$\omega = \mu^2/2\eta \tag{10}$$

$$S = 1/\eta \tag{11}$$

Nonlinear optical effects Nonlinear optical (NLO) parameters such as static dipole moment (μ_o), mean polarizability ($|\alpha_o|$), anisotropy of polarizability ($\Delta\alpha$) and first hyperpolarizability (β_o) of the compounds were calculated using the following Eqs. 12–15 [28]. The first hyperpolarizability (β_o) is a third rank tensor that can be described by a 3 × 3 × 3 matrix. The 27 components of the 3D matrix can be reduced to 10 components due to the Kleinman symmetry [30].

$$\mu_o = \left(\mu_x^2 + \mu_y^2 + \mu_z^2\right) \tag{12}$$

$$\alpha_o = (1/3)\left(\alpha_{xx} + \alpha_{yy} + \alpha_{zz}\right) \tag{13}$$

$$\Delta\alpha = \left\{\left[\left(\alpha_{xx}-\alpha_{yy}\right)^2+\left(\alpha_{yy}-\alpha_{zz}\right)^2+\left(\alpha_{zz}-\alpha_{xx}\right)^2\right]/2\right\}^{1/2} \tag{14}$$

$$\beta_o = \left[\left(\beta_{xxx} + \beta_{xyy} + \beta_{xzz}\right)^2+\left(\beta_{yyy} + \beta_{yzz} + \beta_{yxx}\right)^2 +\left(\beta_{zzz} + \beta_{zxx} + \beta_{zyy}\right)^2\right]^{1/2} \tag{15}$$

Results and discussion

The unsymmetrical ligand **L** and its metal complexes are stable at room temperature in the solid state. **L** is dark red in color and is soluble in organic solvents, such as methanol, ethanol, chloroform, acetonitrile, DMF and DMSO. The metal complexes are obtained as colored crystalline solids. The metal complexes of **L** are soluble in acetonitrile, DMF, DMSO, chloroform and THF. All the metal complexes are sparingly soluble in methanol and ethanol. The analytical data of **L** and its [Co(**L**)], [Ni(**L**)], [Cu(**L**)] and [Zn(**L**)] complexes are given in Table 1.

Table 1 Analytical and physical data of **L** and its metal(II) complexes

Compound	Yield/%	M. Wt	Color	Elemental analysis/%				Molar conductance /Ω^{-1} cm^2 mol^{-1}
				Found/Calcd.				
				C	H	N	M	
L	71	348	Dark red	68.91/68.95	5.82/5.79	16.12/16.08	–	–
[Co(**L**)]	46	405	Brownish red	59.29/59.27	4.41/4.48	13.78/13.82	14.59/14.54	8.6
[Ni(**L**)]	53	405	Brownish yellow	59.33/59.30	4.51/4.48	13.88/13.83	14.48/14.49	5.5
[Cu(**L**)]	66	409	Brownish green	58.52/58.60	4.47/4.43	13.69/13.67	15.48/15.50	5.2
[Zn(**L**)]	62	411	Reddish yellow	58.80/58.33	4.50/4.41	13.68/13.61	15.80/15.88	2.1

Molar conductance

Molar conductance measurement of the metal complexes was taken in DMF (10^{-3} mol dm^{-3}) solutions at room temperature. The molar conductance values of the [Co(**L**)], [Ni(**L**)], [Cu(**L**)] and [Zn(**L**)] complexes are found to be in the range 2.1–8.6 Ω^{-1} cm^2 mol^{-1}; this low molar conductance values (Table 1) propose that the metal complexes are non-electrolytes [31]. Thus, all the metal complexes of **L** are found to be neutral.

Characterization of the ligand and its metal complexes

IR spectra

The IR spectra of **L** and its metal complexes were recorded in the wave number region 4000–400 cm^{-1} (Figure S1), and the important IR spectral data are given in Table 2. The IR spectrum of **L** shows a broad band centered at 3454 cm^{-1}, which is assigned to the combination of –NH vibration of the quinoxaline ring and –OH stretching vibrations of phenolic –OH group in the *o*-acetophenone moiety. The band at 1676 cm^{-1} in the IR spectrum of **L** is assigned to the >C=O stretching frequency of the quinoxaline ring carbonyl group. These two bands suggest the existence of **L** in keto form. This is further supported by NMR spectral studies. The strong band observed at 1650 cm^{-1} is assigned to the benzophenone imino >C=N stretching frequency. In the IR spectra of the metal complexes, this band shows some shift towards low wave number region for about 10–4 cm^{-1}. This confirms the coordination imino group nitrogen atom with the central metal ion in the metal chelates. In the IR spectrum of **L**, another strong band seen at 1566 cm^{-1} is ascribed to azomethine (–HC=N) stretching frequency. This band is shifted to lower wave umber, 1560 cm^{-1}, in the IR spectra of [Ni(**L**)] complex. On the other hand, the azomethine band is shifted to higher wave numbers, 1577, 1573 and 1572 cm^{-1}, in [Co(**L**)], [Cu(**L**)]and [Zn(**L**)] complexes, respectively. This indicates the coordination of azomethine nitrogen atom to metal ion in metal complexes. The absence of bands in ~3500 and 1676 cm^{-1} regions indicate that the ligand exists in iminol form in the metal chelates [32]. Furthermore, this confirms the coordination of phenolic oxygen atom of *o*-acetophenone and quinoxaline moieties through deprotonation. The presence a new set of bands in the metal chelates in the region 1347–1340 cm^{-1} corresponds to the >C–O stretching frequencies. This also confirms the coordination of **L** via two phenolic oxygen atoms through deprotonation. In the IR spectra of metal complexes, appearance of new bands in the region 476–462 and 412–403 cm^{-1} are attributed to M–O and M–N bond stretching frequencies, respectively [33]. Based on the above observations, it is concluded that **L** behaves as a tetradentate ONNO donor ligand in the metal chelates, coordinating through the azomethine and imino group nitrogen and through the deprotonation of

Table 2 FTIR spectral data of **L** and its metal(II) complexes (cm^{-1})

Compound	ν(OH+NH)	ν(HC=N)	ν(C=N)	ν(C=O)	ν(C–O)	ν(M–O)	ν(M–N)
L	3454	1566	1650	1676	–	–	–
[Co(**L**)]	–	1577	1640	–	1344	462	406
[Ni(**L**)]	–	1560	1644	–	1347	470	412
[Cu(**L**)]	–	1570	1643	–	1335	476	409
[Zn(**L**)]	–	1572	1640	–	1347	467	403

phenolic oxygen atoms in the *o*-hydroxyacetophenone and quinoxaline moieties.

Electronic absorption spectra

The electronic absorption spectra of **L** and its metal(II) complexes (Figure S2) were recorded in DMF solution at room temperature. The absorption region, assignment of the absorption bands and proposed geometry of the complexes are given in Table 3. The electronic spectrum of ligand exhibits three bands. The band observed at 35,461 cm^{-1} is due to the π–π^* transition of aromatic rings of ligand. The absorption band at 31,348 cm^{-1} is assigned to the n–π^* of azomethine chromophore. The other low-energy broad band observed at 23,529 cm^{-1} is presumably due to the intraligand charge transfer transition.

The spectrum of [Co(**L**)] complex exhibits transitions at 35,971, 26,316 and 12,771 cm^{-1}. The bands at 35,971 and 26,316 cm^{-1} are attributed to the π–π^* and n–π^* transitions, respectively. The *d*–*d* transition observed at 12,771 cm^{-1} is assignable to the $^4A_2(F) \rightarrow {}^4T_1(P)$ transition corresponding to tetrahedral geometry. The electronic absorption spectrum of [Ni(**L**)] complex exhibits two intraligand charge transfer and one *d*–*d* transition band. The π–π^* transition band is observed at 36,101 cm^{-1}. The absorption band due to n–π^* transition is seen at 23,923 cm^{-1}. The *d*–*d* transition band corresponding to $^3T_1(F) \rightarrow {}^3T_1(P)$ transition is seen at $\sim$18,182 cm^{-1}. This suggests that the Ni(II) complex possesses tetrahedral geometry [34]. The [Cu(**L**)] complex also exhibits three absorption bands. The bands found at 37,037 and 27,855 cm^{-1} are assignable to the π–π^* and n–π^* transitions, respectively. The broad absorption band observed in the 20,000–16,667 cm^{-1} region centered at $\sim$18,108 cm^{-1} is assignable to the $^2B_{1g} \rightarrow {}^2A_{1g}$ transition, corresponding to square planar geometry of the Cu(II) complex [35]. The [Zn(**L**)] complex exhibits only the intraligand charge transfer bands at 32,258 and 23,641 cm^{-1} in its electronic absorption spectrum.

Table 3 Electronic absorption bands and magnetic moments of **L** and its metal(II) complexes

Compound	ν/cm^{-1}	μ_{eff}/BM	Geometry
L	35,461/31,348/23,529	–	–
[Co(**L**)]	35,971/26,316/12,771	4.25	Tetrahedral
[Ni(**L**)]	36,101/23,923/18,182	3.23	Tetrahedral
[Cu(**L**)]	37,037/27,855/18,018	1.88	Square planar
[Zn(**L**)]	32,258/23,641	–	Tetrahedral

Magnetic susceptibility measurements

The μ_{eff} of the metal ions in the metal chelates of **L** was calculated after making proper diamagnetic corrections. The [Co(**L**)] complex has a magnetic moment value 4.25 BM, which is found to be in agreement with the reported values for tetrahedral Co(II) complexes [36]. The [Ni(**L**)] complex has magnetic moment value of 3.23 BM, suggesting a tetrahedral environment around the Ni(II) ion [37]. The [Cu(**L**)] complex possesses magnetic moment value 1.88 BM, which is consistent with the square planar geometry around the Cu(II) ion [38].

^{1}H NMR

The ^{1}H NMR spectrum of **L** is given in Figure S3a. The signal for azomethine proton in **L** appears as a singlet at 7.9 ppm. The other two singlets seen in the ^{1}H NMR spectrum of **L** at 16.4 and 12.2 ppm are assigned to the quinoxaline ring –NH [36] and *o*-hydroxy acetophenone –OH proton [39] resonance, respectively. The multiplet seen in 6.7–7.7 ppm range is due to the aromatic protons of **L** as expected. The *o*-hydroxyacetophenone methyl group proton resonance was observed at 2.6 ppm. The other peaks observed at 3.4, 3.7 and 2.2 ppm are ascribed to the 1,3-diaminopropane group aliphatic proton resonance.

The ^{1}H NMR spectrum of the [Zn(**L**)] complex (Figure S3b) was compared with that of **L**. In the ^{1}H NMR spectrum of [Zn(**L**)] complex, the signals due to quinoxaline ring –NH and *o*-hydroxy acetophenone –OH proton resonance are not observed. This reveals the presence of **L** in its enol form and coordination of two phenolic oxygen atoms through deprotonation. The downfield shift of azomethine proton signal further tells the coordination of azomethine nitrogen atom. The signals due to aromatic and aliphatic protons of 1,3-diaminopropane also show some shift in the ^{1}H NMR spectrum of [Zn(**L**)] complex, due to the change in the electronic environment around these groups on chelation.

^{13}C NMR

In the ^{13}C NMR spectrum of **L** (Figure S4), the signals seen at 164.3 and 172.6 ppm are ascribed to the carbonyl carbon and phenolic >C–O carbon resonance, respectively. The imino group carbon and azomethine carbon resonance are observed at 136.6 and 132.8 ppm, respectively. The signal observed at 130.92 ppm is assigned to the quinoxaline ring >C=N carbon resonance. The aromatic carbon signals are seen at 117.2–128.2 ppm region. The *o*-hydroxyacetophenone group methyl carbon peak is observed at 46.5 ppm. Three different kinds of carbon atoms present

in the 1,3-diaminopropane moiety resonates at 30.9, 26.8 and 14.74 ppm. In the ^{13}C NMR spectrum of [Zn(**L**)] complex, the aliphatic carbon resonance remains almost unchanged. The carbonyl carbon signal is not found in the spectrum of [Zn(**L**)] complex, and a new signal is observed at 170.4 ppm, which indicates the existence of enol form of **L** in the metal chelates. The phenolic >C–O signal shows small shift due to its coordination of the metal ion through deprotonation.

Mass spectrometry

The DART mass spectrum **L** is given in Figure S5. In the mass spectrum of **L**, the molecular ion peak seen at $m/z = 349.3$ with relative intensity 23% matches with the molecular mass [M + 1] of **L**. The base peak observed at $m/z = 175.09$ matches the molecular mass of (M + 1) of 3-hydroxyquinoxaline-2-carboxaldehyde. In addition to these peaks, **L** shows a series of molecular ion peaks at 391.36 (12%), 326.18 (10%), 311.17 (28%), 309.15 (23%), 255.02 (35%), 212.20 (9%), 177.10 (70%) and 114.11 (13%) corresponding to various fragments. In the mass spectra of [Co(**L**)], [Ni(**L**)], [Cu(**L**)] and [Zn(**L**)] complexes, the molecular ion peaks are appeared at 407.21 (M + 2, 16%), 406.36 (M + 1, 8%), 409.91 (M, 12%) and at 413.73 (M + 2, 11%), respectively. The representative mass spectrum of metal complexes is provided in the supplementary file (Figure S6). Similar to **L**, the metal complexes also show several molecular ion peaks corresponding to various fragmentation processes. The observed molecular ion peaks in the mass spectra of the compounds are in good agreement with their proposed structures arrived on the basis of elemental analysis and other spectral techniques.

EPR spectroscopy

The X-band EPR spectra of the [Cu(**L**)] complex recorded in DMSO at liquid nitrogen temperature (77 K) and in the solid state at room temperature (300 K) are given in Figure S7. The calculated ESR parameters of the [Cu(**L**)] complex are given in Table 4. The EPR spectrum of the [Cu(**L**)] complex at 77 K shows four well-resolved hyperfine peaks. The observed values $g_{\|}$ (2.16) > $g_{\perp}$ (2.04) > 2.0027 indicate that the unpaired electron is localized in $d_x^2 - d_y^2$ orbital of the Cu(II) ion [40]. The calculated G value (4.21) states the absence of magnetic interaction between Cu(II) ions in its solid state. The absence of any half-field signal at 1600 G corresponds to $\Delta Ms = \pm 2$ transition, ruling out any magnetic exchange between Cu(II) centers [41].

The calculated α^2 (0.43), β^2 (0.98) and γ^2 (0.93) values are found to be less than unity. In the present investigation, $K_{\perp}(0.42) > K_{\|}(0.40)$ values found for the [Cu(**L**)] complex indicate the presence of substantial in-plane π-bonding [42]. The results of EPR, electronic absorption spectral and magnetic moment measurements suggest that the [Cu(**L**)] complex has square planar geometry. The calculated empirical factor value ($f = (g_{\|}/A_{\|}) = 137.57$) further confirms square planar geometry of the [Cu(**L**)] complex.

Thermal analysis

Thermal analyses of **L** and its metal(II) complexes were done in the temperature range 40–725 °C in nitrogen and air atmosphere. Alumina was used as the reference compound. All the compounds display multistage thermal decomposition pattern in their thermogravimetric curves.

L shows two stages of thermal decompositions (Fig. 1) in the temperature ranges 95–168 and 168–370 °C with DTG peaks at 148 and 255 °C, respectively. The first-stage decomposition (mass loss (%): obs./calcd.: 16.15/15.51) corresponds to the loss of acetophenone moiety from **L**. The final-stage decomposition (mass loss: obs./calcd.: 83.35/83.11) is due to the removal of remaining organic moieties from the ligand. The thermogravimetric curve of [Co(**L**)] complex shows three stages of decomposition. The thermal decomposition of [Co(**L**)] complex occurs (Fig. 2) in the temperature ranges 100–215, 215–495 and 495–675 °C. The corresponding DTG peaks were observed at 162, 274 and 559 °C, respectively. The first-stage mass loss 10.93% (calcd. 12.59%) is due to the loss of *o*-hydroxyacetophenone part from **L**. The second (mass loss: obs./calcd.: 37.55/35.62) and third (mass loss: obs./calcd.: 24.93/25.93) stages of thermal decompositions correspond to the loss of remaining organic moiety from the metal chelate.

Table 4 ESR parameters of [Cu(**L**)] complex

Complex	g tensors			Hyperfine constant × 10^{-4}		Bonding parameters					
[Cu(**L**)]	$g_{\|}$	$g_{\perp}$	g_{iso}	$A_{\|}$	$A_{\perp}$	G	α^2	β^2	γ^2	$K_{\|}$	$K_{\perp}$
At 77 K	2.16	2.04	–	157	65	4.21	0.43	0.98	0.93	0.42	0.40
At 300 K	–	–	2.02	–	–	–	–	–	–	–	–

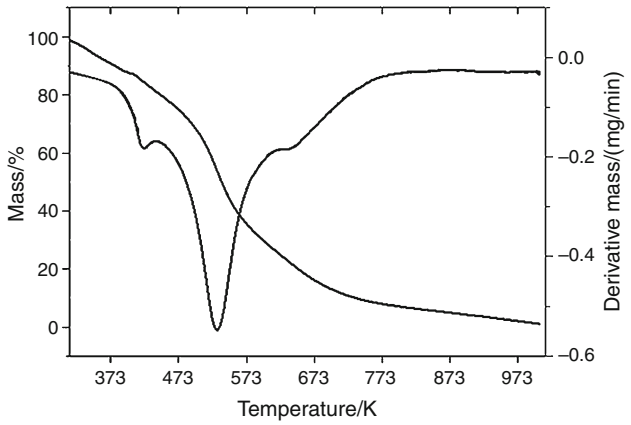

Fig. 1 TG–DTG curves of **L** (*m*: 9.57 mg)

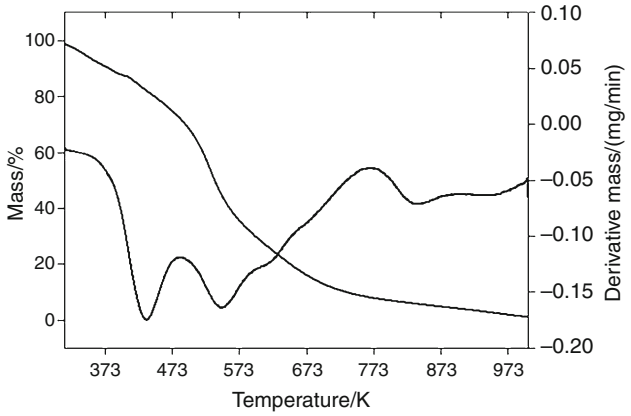

Fig. 2 TG–DTG curves of [Co(**L**)] complex (*m*: 9.71 mg)

The [Ni(**L**)] complex displays three stages of thermal decomposition (Fig. 3). The decompositions of [Ni(**L**)] complex occurs at the temperature ranges 105–268, 268–380 and 380–550 °C with endothermic DTG peaks at 146, 338 and 404 °C, respectively. This first stage of decomposition (mass loss (%): obs./calcd.: 35.76/36.56) corresponds to the removal of *o*-hydroxyacetophenone part from **L**. The second (mass loss (%): obs./calcd.: 15.15/15.19)- and third (mass loss (%): obs./calcd.: 37.55/38.13)-stage decompositions were assigned to the loss of diaminopropane and quinoxaline moieties from the metal chelate.

The [Cu(**L**)] complex shows two stages of thermal decomposition. In the thermogravimetric curve of [Cu(**L**)] complex (Fig. 4), these decompositions were seen at the temperature ranges 110–210 and 210–490 °C. The first-stage decomposition with an endothermic DTG peak at 153 °C (mass loss (%): obs./calcd.: 16.05/16.40) and the second-stage decomposition with an endothermic DTG peak at 238 °C (mass loss (%): obs./calcd.: 55.34/56.64) are because of the loss of organic moieties from the metal complex. The [Zn(**L**)] complex displays two stages of thermal decomposition (Fig. 5) at 110–490 and 490–720 °C range with resultant DTG peaks at 380 and 714 °C, respectively. The first-stage thermal decomposition (mass loss (%): obs./calcd.: 16.05/16.40) corresponds to loss of acetophenone and diaminopropane parts from the metal chelate. The second-stage decomposition (mass loss (%): obs./calcd.: 35.38/37.39) is due the removal of quinoxaline moiety of the [Zn(**L**)] complex.

The thermal analysis of the metal complexes in air atmosphere was also conducted to analyze the metal content. The metal content in the final residues was analyzed by atomic absorption spectroscopy [43]. The final product of [Co(**L**)] complex is observed as CoO residue (obs./calcd.: 18.20/18.49%). The CoO residue is formed after the elimination of organic moieties from the complex at the temperature range 495–675 °C with DTA peak at about 560 °C. The DTA curves of [Ni(**L**)] complex display (Fig. 6) an endothermic peak at 430 °C, due to the loss of organic part and the formation of stable NiO as final product (obs./calcd.: 18.35/18.42%). Likely for the [Cu(**L**)] and [Zn(**L**)] complexes, the final products are found as

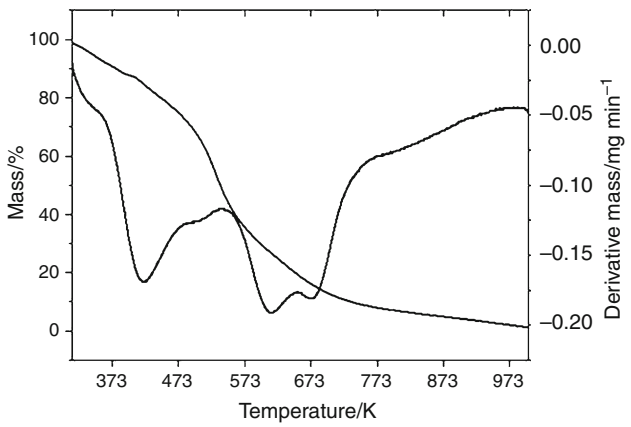

Fig. 3 TG–DTG curves of [Ni(**L**)] complex (*m*: 11.37 mg)

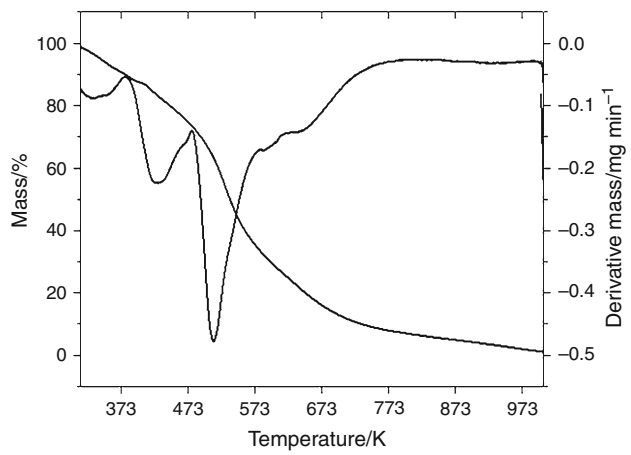

Fig. 4 TG–DTG curves of [Cu(**L**)] complex (*m*: 11.37 mg)

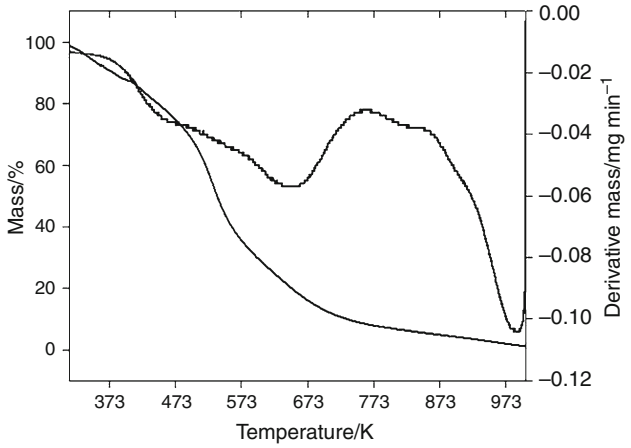

Fig. 5 TG–DTG curves of [Zn(**L**)] complex (*m*: 5.38 mg)

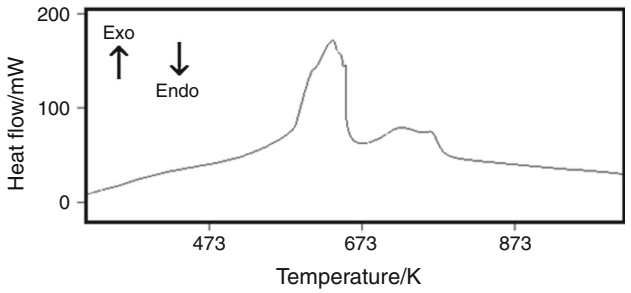

Fig. 6 DTA curve of [Ni(**L**)] complex

stable CuO (obs./calcd.: 19.10/19.40%) and ZnO (obs./calcd.: 19.65/19.76%), respectively.

The proposed structure of metal complexes is given in Scheme 1.

Powder XRD

The powder XRD patterns of **L** and its metal complexes were recorded over the 2θ = 0–80 Å range and are displayed in Figure S8. **L** and its [Cu(**L**)] complex display some crystalline peaks in their XRD diffractogram, while the other metal complexes did not show any peaks. From the powder XRD patterns, we have calculated the average crystallite size and also refined the unit cell parameters. The average crystallite sizes of the compounds are calculated using Scherrer's formula [44]. The calculated average crystallite size of **L** and its [Cu(**L**)] complex is 51.20 and 33.74 nm, respectively. This states that **L** and [Cu(**L**)] complexes are in nanocrystalline phase, while the [Co(**L**)], [Ni(**L**)] and [Zn(**L**)] complexes are amorphous in nature. The refined unit cell parameters of **L** and its [Cu(**L**)] complex are determined using trial and error method and are given in Table S1. **L** and [Cu(**L**)] complex are included in the triclinic crystal system.

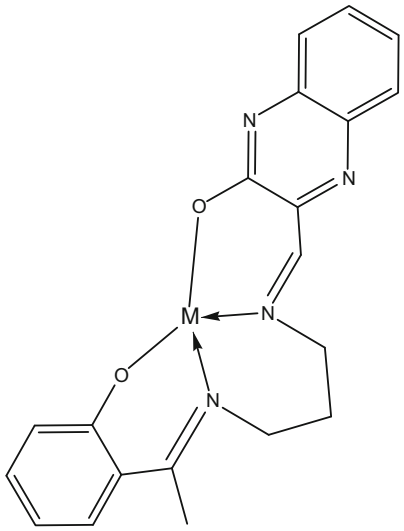

(M = Co(II), Ni(II) and Zn(II))

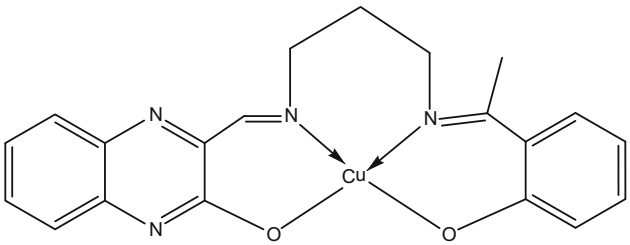

Scheme 1 Proposed structure of metal complexes

Electrochemical analysis

The cyclic voltammograms of the compounds were recorded at 300 K in DMSO solution with scan rate 0.05 V s^{-1}. The potential range was −0.8 to 2.0 V for **L**. For [Co(**L**)], [Ni(**L**)] and [Cu(**L**)] complexes, the potential range was −0.8 to 1.4 V. The potential ranges for [Zn(**L**)] complex was −0.6 to 1.4 V. The cyclic voltammograms of the compounds are given in the supplementary data (Figure S9).

L shows one irreversible cathodic peaks at E_{pc} = −0.42 V versus Ag/AgCl. The [Co(**L**)] complex shows only one irreversible anodic peak at 0.08 V versus Ag/AgCl. This irreversible anodic peak is assignable to the Co(II)/Co(III) oxidation process. The [Ni(**L**)] complex displayed two irreversible peaks versus Ag/AgCl. The first cathodic peak at E_{pc} = −0.68 V corresponds to the Ni(II)/Ni(I) reduction, and the corresponding anodic peak at E_{pa} = 1.18 V corresponds to the Ni(I)/Ni(II) oxidation process [45]. The [Cu(**L**)] complex also shows (Fig. 7) two peaks, the cathodic peak at E_{pc} = 0.04 V versus Ag/AgCl corresponding to the formation of Cu(II)/I couple. The

associated anodic peak was observed at $E_{pa} = 1.00$ V, equivalent to Cu(I)/Cu(II) couple. The peak-to-peak separation ΔE_p is 0.96 V which confirms that the process is irreversible. The [Zn(**L**)] complex shows only one irreversible cathodic peak at $E_{pc} = 0.12$ V versus Ag/AgCl.

Biological studies

Antimicrobial activity

The inhibition efficiencies of **L** and its [Co(**L**)], [Ni(**L**)], [Cu(**L**)] and [Zn(**L**)] complexes were tested against some gram-positive and gram-negative bacterial strains by agar diffusion method. The results obtained in terms of activity index are displayed in Fig. 8. From the figure, it is clear that the [Ni(**L**)] and [Zn(**L**)] complexes do not show any inhibition efficiency against the gram-positive bacterial strains. **L** (46.66%), [Co(**L**)] complex (29.16%) and [Cu(**L**)] complex (33.33%) are active against the gram-positive bacterial strain *S. aureus*. The bacterial strain *S. Pneumoniae* is resistant toward **L** and its metal complexes. The [Co(**L**)] complex does not show any antibacterial activities against the gram-negative bacterial strain *E. coli*. The Cu(II) complex shows highest inhibition efficiency against the gram-negative bacterial strains *E. coli* (36.00%) and *K. Pneumoniae* (39.13%). **L** and its [Co(**L**)] and [Ni(**L**)] complexes are inactive against the gram-negative bacterial strain *K. Pneumoniae*. The compounds follow the order of antibacterial activity as: [Cu(**L**)] > **L** > [Zn(**L**)] > [Cu(**L**)] > [Ni(**L**)].

Moreover, the antimicrobial activity index of **L** and its metal complexes points out that *S. aureus* is the most susceptible bacterium of all tested strains and that the activity is more noticeable on gram-positive bacterial strains. This distinction in sensitivity between gram-positive and gram-negative bacteria might be associated with the dissimilarities in the morphological compositions among these microbes. Gram-negative bacteria have an outer phospholipid membrane carrying the structural lipopolysaccharide components; this makes the cell wall impermeable to antimicrobial substances. Gram-positive bacteria, on the other hand, are more susceptible because they only have an outer peptidoglycan layer which is permeable [46].

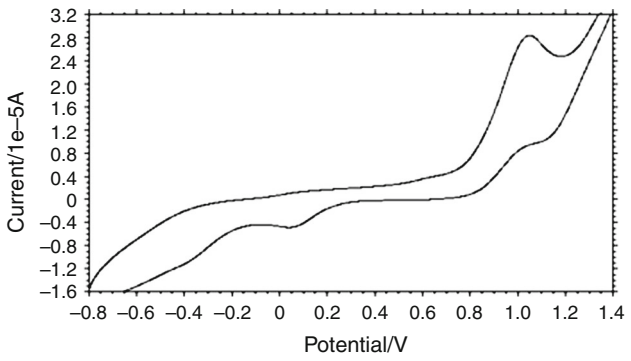

Fig. 7 Cyclic voltammogram of [Cu(**L**)] complex

The antifungal activity screening result is displayed in Fig. 9. From the figure, it is obvious that **L** is active against all the fungal strains under screening. The [Co(**L**)] complex is active against *A. flavus* and *P. chrysogenum*. The [Ni(**L**)] and [Cu(**L**)] complexes are inactive only against the fungal strain *R. stolonifer*; whereas the [Zn(**L**)] complex shows inhibition efficiency only against the fungal strain *A. flavus*. Among the newly synthesized compounds, [Cu(**L**)] complex (47.36%) exhibits higher antifungal activity against *A. niger*. The Co(II) complex shows higher inhibition efficiencies against the fungal strains *A. flavus* (52.17%) and *P. chrysogenum* (80.00%), while **L** shows highest antifungal activity against the fungal strain *R. stolonifer* (50.00%). The order of antifungal activity is as follows: [Co(**L**)] > **L** > [Cu(**L**)] > [Ni(**L**)] > [Zn(**L**)].

The antimicrobial screening of the compounds reveals that the [Cu(**L**)] and [Co(**L**)] complexes have highest antibacterial and antifungal potentials, respectively.

DNA cleavage

The interaction of plasmid pUC18 DNA with **L** and its metal(II) complexes was studied using agarose gel electrophoresis method in the presence of an oxidizing agent (H_2O_2) and in the presence of reactive oxygen species scavenger (DMSO). When a supercoiled circular plasmid DNA is subjected to DNA cleavage study, if scission occurs on one strand (single-stranded nicking), the supercoiled Form I will be relaxed to generate a slow-moving open circular form (Form II). If both strands are cleaved (double-stranded nicking), a linear form (Form III) that migrates between Form I and Form II will be generated [47].

The DNA cleavage studies of the compounds in the presence of H_2O_2 (Fig. 10a) show that except **L**, the metal chelates completely degrade all the three forms of pUC18 DNA. **L** cleaves pUC18 DNA into its open circular form (Form II). This proposes that DNA cleavage process occurs through oxidative cleavage mechanism. In oxidative cleavage mechanism, when redox-active metal complexes interact with DNA in the presence of an oxidizing agent, it is supposed to produce different reactive oxygen species (ROS), depending on specific complex and conditions. A non-diffusible metal-peroxo intermediate has been invoked in some cleavage reactions though in others cases, Fenton-like chemistry, which invokes release of freely diffusible hydroxyl ($OH^{\cdot}$) or hydroperoxyl ($HO^{2\cdot}$) radical, has been assumed. The metal complexes in the presence of H_2O_2

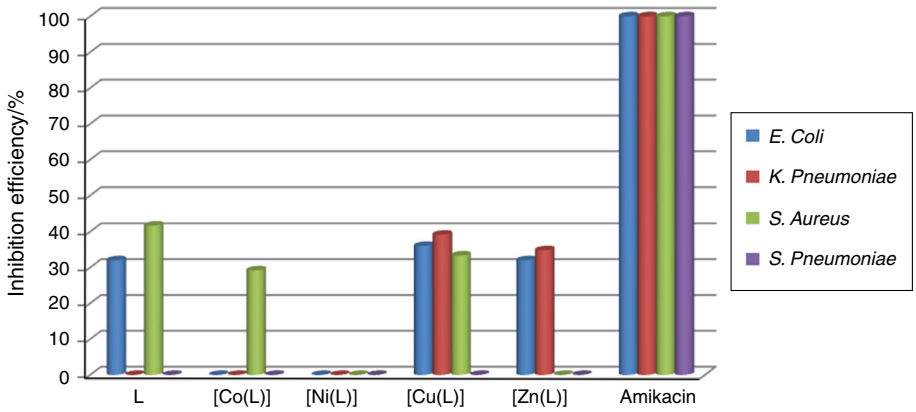

Fig. 8 Antibacterial activity of **L** and its metal(II) complexes

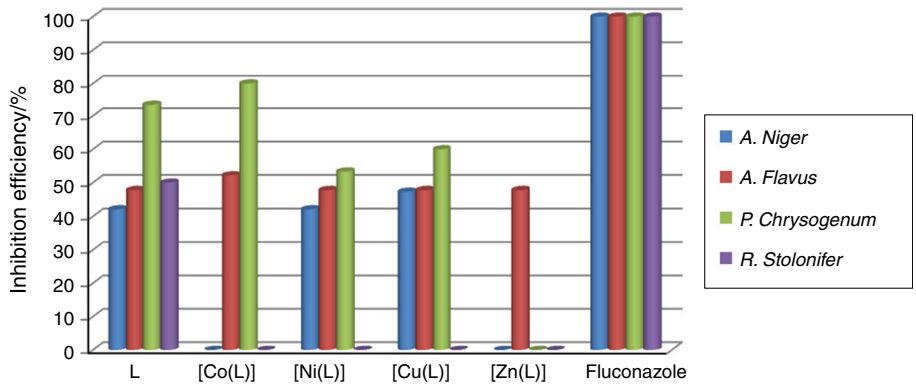

Fig. 9 Antifungal activity of **L** and its metal(II) complexes

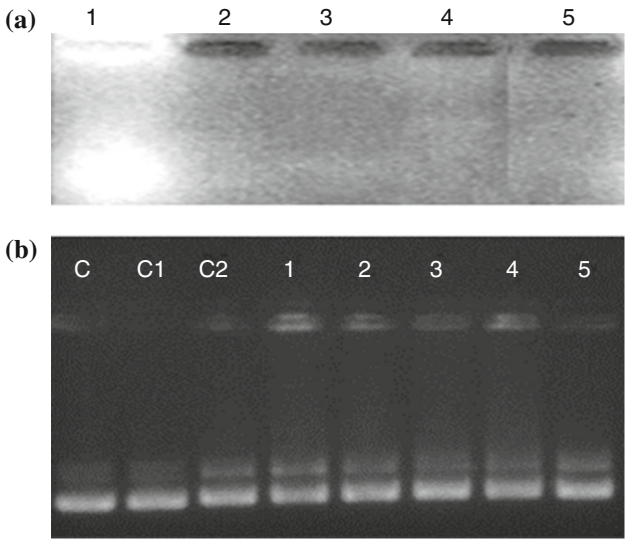

Fig. 10 **a** DNA cleavage activity of **L** and its metal complexes (where *Lanes 1*, *2*, *3*, *4* and *5* are DNA-treated with **L**, [Co(**L**)], [Ni(**L**)], [Cu(**L**)] and [Zn(**L**)] complexes (50 μM) along with 100 μM H_2O_2). **b** DNA cleavage activity of **L** and its metal(II) complexes (where *Lane C*: control DNA (untreated sample), *Lane C1*: DNA with 0.5 μL DMSO, *Lane C2*: DNA with 100 μM H_2O_2, *Lane 1*: **L**+H_2O_2+DMSO, *Lane 2*: [Co(**L**)] complex + H_2O_2 + DMSO, *Lane 3*: [Ni(**L**)] complex+H_2O_2+DMSO, *Lane 4*: [Cu(**L**)] complex + H_2O_2 + DMSO and *Lane 5*: [Zn(**L**)] complex + H_2O_2 + DMSO

may generate reactive hydroxyl/hydroperoxyl radical that can destruct the deoxyribose ring or otherwise a metal-peroxo species may take part directly in the oxidation of deoxyribose ring [48].

To recognize the contribution of ROS, electrophoresis experiment was carried out in the presence DMSO as a standard scavenger for reactive oxygen intermediates under the same experimental conditions. Addition of DMSO results in complete inhibition of the cleavage activity of all the present compounds (Fig. 10b), proposing the possibility of formation of diffusible hydroxyl radical as the reactive species leading to strand scission [49].

Antioxidant activity

Superoxide anion scavenging activity The in vitro superoxide anion scavenging activities of **L** and its metal(II) complexes were evaluated by spectroscopic method using NBT as indicator. The percentage of superoxide anion elimination capabilities of the compounds are displayed in Fig. 11. The results show that the compounds possess moderate superoxide anion scavenging abilities. The inhibition efficiencies of the compounds are in the range 43.36–84.54%. Among the compounds, [Zn(**L**)] and [Cu(**L**)] complexes show highest and lowest superoxide

anion scavenging activities, respectively. **L** shows 63.48% elimination activity of superoxide anions from the reaction mixture. On chelation, **L** with Co(II), Ni(II) and Cu(II) ions slightly lowered its activity, while chelation of **L** with Zn(II) ion enhanced its antioxidant activity. The order of superoxide anion scavenging activity is as follows: [Zn(**L**)] > **L** > [Co(**L**)] > [Ni(**L**)] > [Cu(**L**)].

Hydrogen peroxide scavenging activity The in vitro hydrogen peroxide scavenging activity results (Fig. 12) reveal that the [Co(**L**)] and [Ni(**L**)] complexes have moderate hydrogen peroxide scavenging power. The percentage of hydrogen peroxide elimination activity of **L** and its metal complexes ranges 25.55–62.70%. Among the present compounds, the [Ni(**L**)] complex shows highest and [Cu(**L**)] complex shows lowest hydrogen peroxide scavenging activity. The order of activity is as follows: [Ni(**L**)] > [Co(**L**)] > **L** > [Zn(**L**)] > [Cu(**L**)].

Anticancer activity

The in vitro anticancer activity of the compounds against the human breast adenocarcinoma (MCF7) cell lines was evaluated by MTT assay. The cell viability and the effect of increasing concentration (0.25–100 μM) of the compounds against MCF7 cell line are given in Figures S10 and S11, respectively. The figures pointed out that the anticancer activity of the compounds depends on concentration. As the concentration of compounds increases, the activity also increased. The anticancer activity results of the compounds in terms of IC_{50} values are provided in Table 5. Among the synthesized compounds, the Cu(II) complex has low IC_{50} value and is highly active. **L** and its [Co(**L**)] complex are ineffective, and their IC_{50} values are greater than 100 μM. On comparing the IC_{50} values of the compounds with standard drug (tamoxifen), the compounds are not much effective against the human breast adenocarcinoma cell line.

The enhanced anticancer activity of [Ni(**L**)], [Cu(**L**)] and [Zn(**L**)] complexes compared with the uncoordinated **L** may be ascribed to the increase in conjugation with –R=N–R′ moiety in **L** on chelation. The variation in the cytotoxicity of the metal complexes with the same ligand at a given concentration describes a synergistic effect upon coordination of metal ions. Additionally, improved activity of metal chelates may also be attributed due to higher lipophilic nature of the complexes which increased due to chelation. It is most likely due to fast diffusion of the chelates through the cell membrane or due to the chelation effect [3].

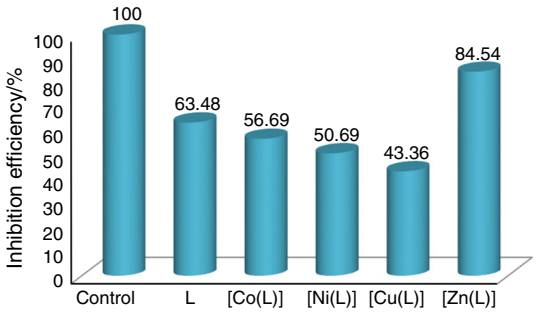

Fig. 11 Superoxide anion scavenging activity of **L** and its metal(II) complexes

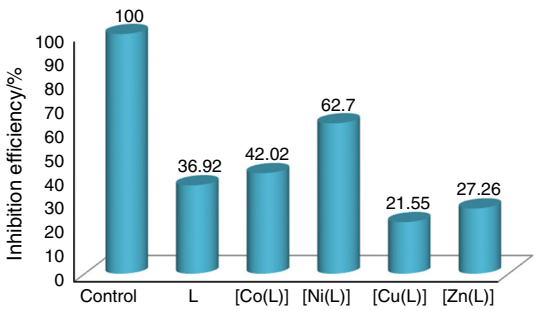

Fig. 12 Hydrogen peroxide scavenging activity of **L** and its metal(II) complexes

DFT studies

Geometry optimization The structure of **L** and its metal(II) chelates was optimized using Gaussian 09 program. B3LYP/6-31G(*d*,*p*) and B3LYP/LANL2DZ basis sets were used for the geometry optimization of **L** and its metal(II) complexes, respectively. The selected bond lengths and bond angles for the compounds are provided in Table 6. The optimized structure of the compounds is depicted in Fig. 13. The optimum energies of **L** and its [Co(**L**)], [Ni(**L**)], [Cu(**L**)] and [Zn(**L**)] complexes are −1143.63, 1287.54, −1311.81, −1338.64 and −1208.11 a.u, respectively. Theses energy values indicate that on chelation, metal chelates become more stable than the **L**. Among the metal complexes, [Ni(**L**)] complex is found to be more stable. From the optimized structures, it is obvious that

Table 5 IC_{50} values of **L** and its metal(II) complexes

Compound	IC_{50}/μM
L	>100
[Co(**L**)]	>100
[Ni(**L**)]	97.03
[Cu(**L**)]	40.39
[Zn(**L**)]	76.53
Tamoxifen[a]	11.20

[a] Standard drug

Table 6 Selected geometrical parameters of **L** and its metal(II) complexes

Bond connectivity	Bond length/Å	Bond connectivity	Bond angle/°
L			
1C–15N	1.3013	3C–14N–4C	124.954
4C–16O	1.2238	14N–4C–16O	121.238
4C–14N	1.3891	1C–17C–19N	130.841
14N–8H	1.0136	19N–20C–23C	109.622
17C–19N	1.2707	20C–23C–26C	112.321
17C–18H	1.0944	26C–29N–30C	121.250
19N–20C	1.4562	25N–30C–31C	125.693
26C–29N	1.4534	31C–30C–35C	116.701
29N–30C	1.2768	30C–35C–37C	122.291
37C–45O	1.3627	37C–45O–46 H	108.522
[Co(**L**)]			
4C–15O	1.2936	13N–4C–15O	119.836
15O–45Co	1.8953	14N–1C–16C	113.312
16C–18N	1.2918	16C–18N–19C	120.316
18N–45Co	2.0883	19C–22C–25C	109.233
28N–29C	1.3044	25C–28N–29C	127.657
28N–45Co	1.9933	30C–29C–34C	119.981
44O–45Co	1.8654	15O–45Co–44O	107.032
36C–44O	1.3041	15O–45Co–18N	90.259
1C–14N	1.3828	44O–45Co–28N	87.245
4C–13N	1.3331	44O–45Co–18N	128.018
[Ni(**L**)]			
4C–15O	1.2870	13N–4C–15O	119.484
15O–45Ni	1.8856	14N–1C–16C	115.208
16C–18N	1.2985	16C–18N–19C	114.215
18N–45Ni	1.9696	19C–22C–25C	112.169
28N–29C	1.3239	25C–28N–29C	118.274
28N–45Ni	1.9565	30C–29C–34C	116.644
44O–45Ni	1.8272	15O–45Ni–44O	107.490
36C–44O	1.2926	15O–45Ni–18N	91.133
1C–14N	1.3314	44O–45Ni–28N	90.631
4C–13N	1.3410	44O–45Ni–18N	119.775
[Cu(**L**)]			
4C–15O	1.2826	13N–4C–15O	119.019
15O–45Cu	1.9407	14N–1C–16C	113.557
16C–18N	1.2924	16C–18N–19C	118.236
18N–45Cu	2.0194	19C–22C–25C	115.454
28N–29C	1.3143	25C–28N–29C	117.783
28N–45Cu	2.0627	30C–29C–34C	116.998
44O–45Cu	1.8990	15O–45Cu–44O	91.424
36C–44O	1.2826	15O–45Cu–18N	92.122
1C–14N	1.3316	44O–45Cu–28N	90.031
4C–13N	1.3425	44O–45Cu–18N	90.132
[Zn(**L**)]			
4C–15O	1.2887	13N–4C–15O	118.906
15O–45Zn	1.9466	14N–1C–16C	112.327
16C–18N	1.2931	16C–18N–19C	117.018
18N–45Zn	2.1176	19C–22C–25C	115.648
28N–29C	1.3075	25C–28N–29C	122.251
28N–45Zn	2.0850	30C–29C–34C	118.071
44O–45Zn	1.9400	15O–45Zn–44O	115.967
36C–44O	1.3088	15O–45Zn–18N	92.990
1C–14N	1.3320	44O–45Zn–28N	91.133
4C–13N	1.3377	44O–45Zn–18N	133.593

L acts as a tetradentate ligand and coordinates with the metal ions through two nitrogen atoms: one from azomethine and another from imine groups, through phenolic oxygen atom of quinoxaline ring through deprotonation and through phenolic oxygen atom of acetophenone moiety through deprotonation. The ligand-to-metal ratio is found to be 1:1. The [Co(**L**)], [Ni(**L**)] and [Zn(**L**)] metal complexes possess tetrahedral geometry, while the [Cu(**L**)] complex possesses square planar geometry.

Frontier molecular orbitals The highest occupied molecular orbital (HOMO) and the lowest unoccupied molecular orbital (LUMO) energy portrays the capability of electron-donating and electron-accepting properties of a compound. These orbitals are a pair of orbitals in the compound, which allows them to interact more strongly. HOMOs and LUMOs are sometimes titled as frontier molecular orbitals (FMOs), for the reason that they lie at the outmost boundaries of the electrons of compounds. The frontier molecular orbitals play a vital role in the optical and electrical properties. The frontier orbital energy gaps also help to illustrate the kinetic stability and the chemical reactivity of a compound. A molecule with a small frontier orbital gap is generally associated with high chemical reactivity and low kinetic stability and is also termed as soft molecule [50].

The energies for second highest occupied molecular orbital (HOMO-1), the highest occupied molecular orbital (HOMO), the lowest unoccupied molecular orbital (LUMO) and the second lowest unoccupied molecular orbital (LUMO+1) were calculated for **L** and its [Co(**L**)], [Ni(**L**)], [Cu(**L**)] and [Zn(**L**)] complexes, and the values are given in Table 7. The energy gap between [HOMO–LUMO] for **L** and its [Co(**L**)], [Ni(**L**)], [Cu(**L**)] and [Zn(**L**)] complexes is −0.23555, −0.11204, −0.10927, −0.12788 and −0.00574 a.u, respectively. From the FMO values, some global reactivity parameters such as absolute electronegativity (χ_{abs}), absolute hardness (η), electrophilicity index (ω) and global softness (S) were calculated using the equations given in the experimental section

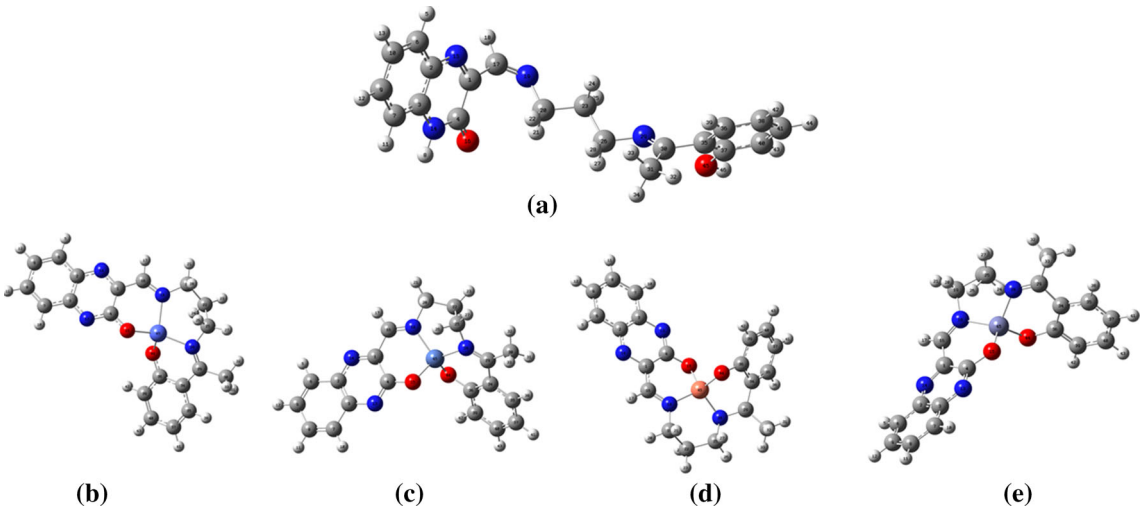

Fig. 13 Optimized structure of **a L**, **b** [Co(**L**)], **c** [Ni(**L**)], **d** [Cu(**L**)] and **e** [Zn(**L**)] complexes

Table 7 Frontier molecular orbital parameters, absolute electronegativity (χ_{abs}), absolute hardness (η), chemical potential (μ), electrophilicity index (ω), global and softness (S) values of **L** and its metal(II) complexes

Parameters/eV	**L**	[Co(**L**)]	[Ni(**L**)]	[Cu(**L**)]	[Zn(**L**)]
[HOMO − 1]	−0.23527	−0.19511	−0.20503	−0.09255	−0.22465
HOMO	−0.23364	−0.19568	−0.19386	−0.22229	−0.10600
LUMO	0.00191	−0.08364	−0.08459	−0.09441	−0.10026
[LUMO + 1]	0.00622	−0.08184	−0.06679	−0.09206	−0.01207
[HOMO–LUMO]	−0.23555	−0.11204	−0.10927	−0.12788	−0.00574
{[HOMO − 1] − [LUMO + 1]}	−0.24149	−0.11327	−0.13824	−0.00049	−0.21258
χ_{abs}	0.1158	0.1396	0.1392	0.1583	0.1031
μ	−0.1158	−0.1396	−0.1392	−0.1583	−0.1031
η	0.1177	0.0560	0.0546	0.0639	0.0028
ω	0.0569	0.1740	0.1773	0.1960	1.8529
S	4.2453	8.9253	9.1516	7.8198	174.2160

and are given in Table 7. The molecules having a large energy gap are known as hard molecules, and molecules having a small energy gap are known as soft molecules. The soft molecules are more polarizable than the hard ones because they need small energy for excitation [51]. The calculated absolute hardness values suggest that **L** and its metal complexes are moderately hard materials. The higher biological activities of the metal compounds are ascribed to their low hardness values.

Atomic charge analysis The Mulliken and natural atomic charge distributions in **L** and its [Co(**L**)], [Ni(**L**)], [Cu(**L**)] and [Zn(**L**)] complexes were analyzed by B3LYP/6-31G(*d*,*p*) and B3LYP/LANL2DZ basis sets, respectively. All the nitrogen and oxygen atoms in **L** have negative atomic charges in both Mulliken and natural atomic charge analyses, while all hydrogen atoms possess positive charges. The carbon atoms C(6), C(7), C(8), C(9), C(10), C(20), C(23), C(26), C(31), C(36), C(38), C(40) and C(41) hold negative Mulliken and atomic charges. The carbon atom C(35) display positive Mulliken and negative natural atomic charges. The atomic charge analysis results of **L** and its complexes are given in Table S2-S6. Atomic charge analyses of metal complexes reveal that all the metal complexes show more or less comparable charge distributions. Mulliken and negative natural atomic charge analyses show that all the metal ions and hydrogen atoms have positive and all oxygen and nitrogen atoms have negative charges. In [Co(**L**)], [Ni(**L**)], [Cu(**L**)] and [Zn(**L**)] complexes, the carbon atoms C(6), C(7), C(8), C(9), C(19), C(22), C(25), C(30), C(35), C(37), C(39) and C(40) display negative Mulliken and natural atomic charges. In the Co(II), Ni(II) and Cu(II) complexes, the C(34) atom bears positive Mulliken and negative natural atomic charges. In

Table 8 Calculated dipole moment (μ_o), polarizability ($|\alpha_o|$), anisotropy of polarizability ($\Delta\alpha_o$), first hyperpolarizability (β_o) and its components using B3LYP/6-31G(*d*,*p*) basis set for **L** and B3LYP/LANL2DZ basis set for the metal(II) complexes of **L**

Parameter	**L**	[Co(**L**)]	[Ni(**L**)]	[Cu(**L**)]	[Zn(**L**)]
Dipole moment					
μ_x	−2.6827	−4.0641	−4.1075	−3.6155	1.8039
μ_y	3.7182	−5.5994	−5.1994	6.3138	6.5642
μ_z	2.8288	0.6463	0.2980	−1.1121	1.1632
μ_o	5.3874	6.9490	6.6328	7.3602	6.9062
Polarizability					
α_{xx}	−99.0691	−130.7546	−128.8761	−134.4598	−140.0679
α_{yy}	−148.4995	−138.2736	−137.4350	−142.5087	−145.3055
α_{zz}	−147.9733	−167.3948	−167.3509	−164.0784	−159.9372
$\|\alpha_o\|$	19.5397	21.5592	21.4229	21.7877	21.9983
$\Delta\alpha_o$	49.1694	33.5192	34.9894	26.5263	17.8369
Hyperpolarizability					
β_{xxx}	−5.8808	−19.4816	−26.4275	−25.0613	−31.3048
β_{xxy}	21.7011	17.6789	17.7719	−2.5880	−14.4548
β_{xyy}	35.6816	−37.6196	−39.1918	−42.6021	37.8918
β_{yyy}	2.7223	−54.8577	−54.1846	43.9378	47.5285
β_{xxz}	41.3789	32.4690	29.2586	−32.4610	41.8182
β_{xyz}	−14.5658	15.5444	14.7717	2.3287	14.1279
β_{yyz}	−4.8107	−6.7373	−4.9757	8.7606	−15.2494
β_{xzz}	−41.7371	−24.2611	−22.7992	−22.3641	27.9643
β_{yzz}	5.9442	−13.2677	−14.5057	17.0256	13.9403
β_{zzz}	31.3456	5.1598	4.0714	13.5104	−14.0661
β_o	0.6508	0.8690	0.9148	0.9311	0.5151

μ_o in Debye; $|\alpha_o|$ and $\Delta\alpha_o$ in 10^{-24} esu; β_o in 10^{-30} esu

[Zn(**L**)] complex, the C(34) atom possesses negative charge in both Mulliken and natural atomic charges.

Nonlinear optical effects To understand the NLO effects of **L** and its metal complexes, the NLO parameters such as static dipole moment (μ_o), mean polarizability ($|\alpha_o|$), anisotropy of polarizability ($\Delta\alpha$) and first hyperpolarizability (β_o) were calculated using the equations given in the experimental section.

The values calculated using DFT are given in Table 8. The general ranking of NLO properties of the compounds is as follows:

[Zn(**L**)] > [Cu(**L**)] > [Co(**L**)] > [Ni(**L**)] > **L** (based on $|\alpha_o|$ value)
L > [Ni(**L**)] > [Co(**L**)] > [Cu(**L**)] > [Zn(**L**)] (based on $\Delta\alpha$ value)
[Cu(**L**)] > [Ni(**L**)] > [Co(**L**)] > **L** > [Zn(**L**)]) (based on β_o value)

In the meantime, there is no experimental hyperpolarizability (β_o) values available for the present compounds; hence, the calculated values of the compounds were compared with that of urea ($\beta_o = 0.37 \times 10^{-30}$ esu) [52]. This value is compared with that of **L** and its metal complexes; they show a number of times greater hyperpolarizability values than that of urea. From this, we can conclude that the compounds are better NLO candidates.

Conclusions

The unsymmetrical ligand 3-(-(3-(-1-(2-hydroxyphenyl)ethylideneamino)propylimino)methyl)quinoxalin-2(1*H*)-one (**L**) and its Co(II), Ni(II), Cu(II) and Zn(II) complexes have been synthesized and characterized by spectral and analytical methods. From the studies, following conclusions are drawn. The molar conductance values of the metal complexes are found to be in the range 2.1–8.6 Ω^{-1} cm^2 mol^{-1}. This shows that the metal complexes of **L** are non-electrolytes. FTIR spectral study gave vital information about the coordination behavior of **L**. **L** coordinates with the metal ions through the azomethine and imine group nitrogen atoms and through the deprotonation of phenolic oxygen atoms in the *o*-hydroxyacetophenone

and quinoxaline moieties. Tetrahedral geometry is proposed for the [Co(**L**)], [Ni(**L**)] and [Zn(**L**)] complexes, whereas square planar geometry has been assigned for the [Cu(**L**)] complex. Thermal analysis reveals that the metal complexes are thermally more stable than **L**. The order of thermal stability is as follows: [Cu(**L**)] = [Zn(**L**)] > [Ni(**L**)] > [Co(**L**)] > **L**. From the analytical, spectral and thermal studies, the following general formula is assigned to the metal complexes [M(**L**)].

Electrochemical studies using cyclic voltammetry show that the metal(II) complexes are electrochemically active. From powder XRD analysis, it is concluded that **L** and its [Cu(**L**)] complex are in nanocrystalline phase, while Co(**L**), Ni(**L**) and Zn(**L**) complexes are amorphous in nature. Average crystallite size calculated for **L** and its Cu(II) complex is 51.20 and 33.74 nm, respectively. The in vitro biological assays show that the [Cu(**L**)] complex has highest antibacterial activity. The order of antibacterial activity of **L** and its metal complexes is as follows: [Cu(**L**)] > **L** > [Zn(**L**)] > [Co(**L**)] > [Ni(**L**)]. The [Co(**L**)] complex exhibits highest antifungal activity. The DNA binding affinity of **L** and its metal(II) complexes follows the order [Zn(**L**)] > **L** > [Cu(**L**)] > [Ni(**L**)] > [Co(**L**)]. DNA cleavage study suggests that the DNA cleavage process occurs through oxidative cleavage mechanism. The in vitro antioxidant studies reveal that the [Zn(**L**)] and [Ni(**L**)] complexes possess highest superoxide anion and hydrogen peroxide scavenging activities, respectively. In anticancer study, the [Cu(**L**)] complex has lowest IC_{50} value (40.39 μM) and is highly active. Molecular docking studies are in accordance with the DNA binding and MTT assay results. DFT studies indicate that **L** and its metal(II) complexes are good NLO material candidates.

Acknowledgements The authors gratefully acknowledge Dr. T. F. Abbs Fen Reji, Asst. Professor, Department of Chemistry, NMCC, Marthandam, for DFT studies.

References

1. Temel E, Alaşalvar C, Gokce H, Guder A, Albayrak C, Alpaslan YB, Alpaslan G, Dilek N. DFT calculations, spectroscopy and antioxidant activity studies on (*E*)-2-nitro-4-[(phenylimino)methyl]phenol. Spectrochim Acta A. 2015;136:534–46.
2. Zafar H, Ahmad A, Khan AU, Khan TA. Synthesis, characterization and antimicrobial studies of Schiff base complexes. J Mol Struct. 2015;1097:129–35.
3. Shakir M, Hanif S, Sherwani MA, Mohammad O, Al-Resayes SI. Pharmacologically significant complexes of Mn(II), Co(II), Ni(II), Cu(II) and Zn(II) of novel Schiff base ligand (E)-*N*-(furan-2-yl methylene) quinolin-8-amine: synthesis, spectral, XRD, SEM, antimicrobial, antioxidant and in vitro cytotoxic studies. J Mol Struct. 2015;1092:143–59.
4. Parrilha GL, Ferraz KSO, Lessa JA, Oliveira KN, Rodrigues BL, Ramos JP, Souza-Fagundes EM, Ott I, Beraldo H. Metal complexes with 2-acetylpyridine-*N*(4)-orthochlorophenylthiosemicarbazone: cytotoxicity and effect on the enzymatic activity of thioredoxin reductase and glutathione reductase. Eur J Med Chem. 2014;84:537–44.
5. Sanghamitra NJ, Phatak P, Das S, Samuelson AG, Somasundaram K. Mechanism of cytotoxicity of copper(I) complexes of 1,2-bis(diphenylphosphino)ethane. J Med Chem. 2005; 48:977–85.
6. Budagumpi S, Kulkarni NV, Kurdekar GS, Sathisha MP, Revankar VK. Synthesis and spectroscopy of Co(II), Ni(II), Cu(II) and Zn(II) complexes derived from 3,5-disubstituted-1H-pyrazole derivative: a special emphasis on DNA binding and cleavage studies. Eur J Med Chem. 2010;45:455–62.
7. Galal SA, Abdelsamie AS, Tokuda H, Suzuki N, Lida A, ElHefnawi MM, Ramadan RA, Atta MHE, El Diwani HI. Part I: synthesis, cancer chemopreventive activity and molecular docking study of novel quinoxaline derivatives. Eur J Med Chem. 2011;46:327–40.
8. Galal SA, Abdelsamie AS, Soliman SM, Mortier J, Wolber G, Ali MM, Tokuda H, Suzuki N, Lida A, Ramadan RA, El Diwani HI. Design, synthesis and structure-activity relationship of novel quinoxaline derivatives as cancer chemopreventive agent by inhibition of tyrosine kinase receptor. Eur J Med Chem. 2013;69:115–24.
9. Galal SA, Khairat SHM, Ragab FAF, Abdelsamie AS, Ali MM, Soliman SM, Mortier J, Wolber G, El Diwani HI. Design, synthesis and molecular docking study of novel quinoxalin-2(1H)-ones as anti-tumor active agents with inhibition of tyrosine kinase receptor and studying their cyclooxygenase-2 activity. Eur J Med Chem. 2014;86:122–32.
10. Ajani OO, Obafemi CA, Nwinyi OC, Akinpelu DA. Microwave assisted synthesis and antimicrobial activity of 2-quinoxalinone-3-hydrazone derivatives. Bioorg Med Chem. 2010;18:214–21.
11. Dhanaraj CJ, Johnson J, Joseph J, Joseyphus RS. Quinoxaline-based Schiff base transition metal complexes: review. J Coord Chem. 2013;66:1416–50.
12. Ray A, Rosair GM, Kadam R, Mitra S. Three new mono–di–trinuclear cobalt complexes of selectively and non-selectively condensed Schiff bases with N2O and N_2O_2 donor sets: syntheses, structural variations. EPR and DNA binding studies. Polyhedron. 2009;28:796–806.
13. Romanowski G, Wera M. Mononuclear and dinuclear chiral vanadium(V) complexes with tridentate Schiff bases derived from *R*(–)-1,2-diaminopropane: synthesis, structure, characterization and catalytic properties. Polyhedron. 2010;29:2747–54.
14. Bauer AW, Kirby WMM, Sherries JC, Truck M. Antibiotic susceptibility testing by a standardized single disk method. Am J Clin Pathol. 1966;45:493–6.
15. Mahapatra BB, Chaulia S, Sarangi AK, Dehury S, Panda J. Synthesis, characterisation, spectral, thermal, XRD, molecular modeling and potential antibacterial study of metal complexes containing octadentate azodye ligands. J Mol Struct. 2015;1087:11–25.
16. Beauchamp C, Fridovich I. Superoxide dismutase: improved assays and an assay applicable to acrylamide gels. Anal Biochem. 1971;44:276–7.
17. Pick E, Keisari YA. Simple colorimetric method for the measurement of hydrogen peroxide produced by cells in culture. J Immunol Methods. 1980;38:161–70.
18. Mosmann T. Rapid colorimetric assay for cellular growth and survival: application to proliferation and cytotoxicity assays. J Immunol Methods. 1983;65:55–63.

19. Monks A, Scudiero D, Skehan P, Shoemaker R, Paull K, Vistica D, Hose C, Langley J, Cronise P, Vaigro-Wolff A, Gray-Goodrich M, Campbell H, Mayo JB. Feasibility of a high-flux anticancer drug screen using a diverse panel of cultured human tumor cell lines. J Natl Cancer Inst. 1991;83:57–766.
20. Frisch MJ et al. Gaussian, Inc. (2013).Wallingford CT.
21. Keith T, Millam J. GaussView, Version 5. (2009). Roy Dennington, Semichem Inc. Shawnee Mission KS.
22. Becke MAD. Density-functional exchange-energy approximation with correct asymptotic behavior. Phys Rec B. 1988;38:3098–100.
23. Lee C, Yang W, Parr RG. Development of the Colle-Salvetti correlation-energy formula into a functional of the electron density. Phys Rev B. 1988;37:785–9.
24. Güveli Ş, Özdemir N, Bal-Demirci T, Ülküseven B, Dincer M, Andac Ö. Quantum-chemical, spectroscopic and X-ray diffraction studies on nickel complex of 2-hydroxyacetophenone thiosemicarbazone with triphenylphospine. Polyhedron. 2010;29:2393–403.
25. Karakaş D, Sayin K. DFT and TD-DFT studies on copper(II) complexes with tripodal tetramine ligands. Indian J Chem. 2013;52A:480–5.
26. Brabec CJ, Sariciftci NS, Hummelen JC. Plastic Solar Cells. Adv Funct Mater. 2001;11:15–26.
27. Ebenso E, Arslan T, Kandemirl F, Love I, Saracoglu M, Umoren SA. Theoretical studies of some sulphonamides as corrosion inhibitors for mild steel in acidic medium. Int J Quantum Chem. 2010;110:2614–36.
28. Govindasamy P, Gunasekaran S. Quantum mechanical calculations and spectroscopic (FT-IR, FT-Raman and UV) investigations, molecular orbital, NLO, NBO, NLMO and MESP analysis of 4-[5-(4-methylphenyl)-3-(trifluoromethyl)-1H-pyrazol-1-yl] benzene-1-sulfonamide. J Mol Struct. 2015;1081:96–109.
29. Maurya RC, Malik BA, Mir JM, Sharma AK. Synthesis, characterization, thermal behavior, and DFT aspects of some oxovanadium(IV) complexes involving ONO-donor sugar Schiff bases. J Coord Chem. 2014;67:3084–106.
30. Kleinman DA. Nonlinear dielectric polarization in optical media. Phys Rev. 1962;126:1977–9.
31. Geary WJ. The use of conductivity measurements in organic solvents for the characterisation of coordination compounds. Coord Chem Rev. 1971;7:81–122.
32. Kulkarni NV, Revankar VK, Kirasur BN, Huger MH. Transition metal complexes of thiosemicarbazones with quinoxaline hub: an emphasis on antidiabetic property. Med Chem Res. 2012;21:663–71.
33. Belal AAM, El-Deen IM, Farid NY, Zakaria R, Refat MS. Synthesis, spectroscopic, coordination and biological activities of some transition metal complexes containing ONO tridentate Schiff base ligand. Spectrochim Acta A. 2015;149:771–87.
34. Lever ABP. Inorganic electronic spectroscopy. 2nd ed. New York: Elsevier; 1968.
35. Regupathy S, Nair MS. Studies on the mixed ligand complexes of copper(II) involving a sulfa drug and some potentially bi or tridentate ligands under physiological conditions. Arab J Chem. 2014;7:1003–12.
36. Alan I, Kriza A, Olar R, Stanica N, Badea M. Spectral, magnetic and thermal characterisation of new Co(II), Ni(II) and Cu(II) complexes with Schiff base 5-bromo-N, N0-bis-(salicylidene)-o-tolidine. J Therm Anal Calorim. 2013;111:1163–71.
37. Banerjea D. Coordination chemistry. India: Tata McGraw-Hill; 1993.
38. Abdel-Kader NS, Amin RM, El-Ansary AL. Complexes of Schiff base of benzopyran-4-one derivative: synthesis, characterization, non-isothermal decomposition kinetics and cytotoxicity studies. J Therm Anal Calorim. 2016;123:1695–706.
39. Kulkarni NV, Bevinhalli NH, Revankar VK. Ligational behavior of S, N, and O donor quinoxaline derivatives toward the later first-row transition metal ions. J Coord Chem. 2010;63:1785–94.
40. Mohanan K, Thankamony M, Kumari BS. Synthesis, spectroscopic characterization, and thermal decomposition kinetics of some lanthanide(III) nitrate complexes of 2-(N-*o*-hydroxyacetophenone)amino-3-carboxyethyl-4,5,6,7-tetrahydrobenzo[b]thiophene. J Rare Earth. 2008;26:463–8.
41. Raman N, Jeyamurugan R, Rani RU, Baskaran T, Mitu L. Synthesis, characterization, DNA binding, oxidative damage of DNA strand scission, and antimicrobial activities of β-diketone condensed Schiff-base transition metal complexes. J Coord Chem. 2010;63:629–1644.
42. Mahmoud WH, Mahmoud NF, Mohamed GG, El-Sonbati AZ, El-Bindary AA. Ternary metal complexes of guaifenesin drug: synthesis, spectroscopic characterization and in vitro anticancer activity of the metal complexes. Spectrochim Acta A. 2015;150:451–60.
43. Dametto PR, Ambrozini B, Caires FJ, Franzini VP, Ionashiro M. Synthesis, characterization and thermal behaviour of solid-state compounds of folates with some bivalent transition metals ions. J Therm Anal Calorim. 2014;115:161–6.
44. Tabassum S, Zaki M, Arjmand F, Ahmad I. Synthesis of heterobimetallic complexes: in vitro DNA binding, cleavage and antimicrobial studies. J Photochem Photobiol B. 2012;114:108–18.
45. Ibrahim MM, Mersal GAM, Al-Juaid S, El-Shazly SA. Syntheses, characterization, and SOD activity studies of barbital-based nickel(II) complexes with different chelating amines: the X-ray crystal structures of Barb-H and $[Ni(Barb)_2(en)_2]$ (Barb = 5,5-diethylbarbiturate). J Mol Struct. 2014;1056–1057:166–75.
46. Charef N, Sebti F, Arrar L, Djarmouni M, Boussoualim N, Baghiani A, Khennouf S, Ourari A, AlDamen MA, Mubarak MS, Peters DG. Synthesis, characterization, X-ray structures, and biological activity of some metal complexes of the Schiff base 2,2′-(((azanediylbis(propane-3,1-diyl))bis(azanylylidene))bis(methanylylidene))diphenol. Polyhedron. 2015;85:450–6.
47. Chaviara AT, Kioseoglou EE, Pantazaki AA, Tsipis AC. Karipidis PA. Kyriakidis DA, Bolos CA. DNA interaction studies and evaluation of biological activity of homo- and hetero-trihalide mononuclear Cu(II) Schiff base complexes. Quantitative structure–activity relationships. J Inorg Biochem. 2008;102:1749–64.
48. Rahiman K, Gurumoorthy P, Mahendiran D, Parbhu D, Arulvasu C. Magneto-structural correlation, antioxidant, DNA interaction and growth inhibition activities of new chloro-bridged phenolate complexes. RSC Adv. 2014;4:42855–72.
49. Dhar S, Nethaji M, Chakravarty AR. DNA cleavage on photoexposure at the d–d band in ternary copper(II) complexes using red-light laser. Inorg Chem. 2006;45:11043–50.
50. Demircioğlu Z, Albayrak C, Buyukgungor O. Theoretical and experimental investigation of (E)-2-([3,4-dimethylphenyl)imino]methyl)-3-methoxyphenol: enol–keto tautomerism, spectroscopic properties, NLO, NBO and NPA analysis. J Mol Struct. 2014;1065–1066:210–22.
51. Suresh S, Gunasekaran S, Srinivasan S. Vibrational spectra (FT-IR, FT-Raman), frontier molecular orbital, first hyperpolarizability, NBO analysis and thermodynamics properties of Piroxicam by HF and DFT methods. Spectrochim Acta A. 2015;138:447–9.
52. Leela JS, Hemamalini R, Muthu S, Al-Saadi AA. Spectroscopic investigation (FTIR spectrum), NBO, HOMO-LUMO energies, NLO and thermodynamic properties of 8-methyl-*N*-vanillyl-6-nonenamideby DFT methods. Spectrochim Acta A. 2015;146:177–86.